Morphological Population Balance for Modeling Crystal Growth in Face Directions

Cai Y. Ma, Xue Z. Wang, and Kevin J. Roberts
Institute of Particle Science and Engineering, School of Process, Environmental and Materials Engineering, University of Leeds, Leeds LS2 9JT, U.K.

DOI 10.1002/aic.11365
Published online December 3, 2007 in Wiley InterScience (www.interscience.wiley.com).

A morphological (or polyhedral) population balance (PB) model is presented for modeling the dynamic size evolution of crystals grown from solution in all crystal growth directions. The morphological PB approach uses the crystal shape information for a single crystal obtained from morphology prediction, or experiment as the initial face locations, as well as face growth rates to predict the shape evolution of the crystal population. For each time instant during the crystallization process, the prediction uses its shape at the previous time moment, and the growth rate for the specific crystal habit plane. The methodology is demonstrated through a study of potash alum ($KAl(SO_4)_2{\cdot}12H_2O$), for which literature data is available for comparison and validation. The discretization method, method of classes, was used to convert the equations to ordinary differential form with the computational domain being discretized into small meshes. The ordinary differential equations (>1.5 million) were then solved simultaneously using the Runge-Kutta-Fehlbergh 4th/5th-order solver with automatic time-step control. The results obtained clearly demonstrate that the morphological PB model developed can predict crystal growth and surface area of individual habit faces in detail, together with crystal shape and size evolution. © 2007 American Institute of Chemical Engineers *AIChE J,* 54: 209–222, 2008

Keywords: morphological population balance, crystal morphology, crystal growth, potash alum ($KAl(SO_4)_2{\cdot}12H_2O$), shape control

Introduction

Products obtained through crystallization from solution often have specific crystal shape and size distributions, which are very important properties due to the fact that they can impact on the downstream processing, final product properties and end-use performance. Crystal morphology prediction therefore has been a very important research area for some time, and there are now in-house and commercial programmes available for research into morphology prediction, for example Cerius[2],[1] HABIT95,[2–4] MORANG,[5] POLYPACK[6] and SHAPE.[7] However, the work has been limited to shape prediction for single crystals rather than for all the crystal population within a process reactor. On the other hand, population balance modeling of the evolution of crystal-size distribution with time in a reactor has mainly been restricted to using a monosize definition, e.g., the volume equivalent diameter of sphere. d_{eq} as defined in Figure 1. This simplified treatment could have the potential to lead to the loss of important product information, notably on crystal shape and its temporal evolution. As illustrated by Figure 1, two crystals with completely different shapes can, in principle, have the same volume equivalent diameter. Furthermore, with the same d_{eq}, the surface areas from crystals with different shapes may vary by a significant degree, e.g., the ratio of surface areas between a cube and a needle in Figure 1a is about 1:6 (Figure 1b), which will almost certainly affect the accurate estimation of many important properties related to

Correspondence concerning this article should be addressed to X. Z. Wang at x.z.wang@leeds.ac.uk.

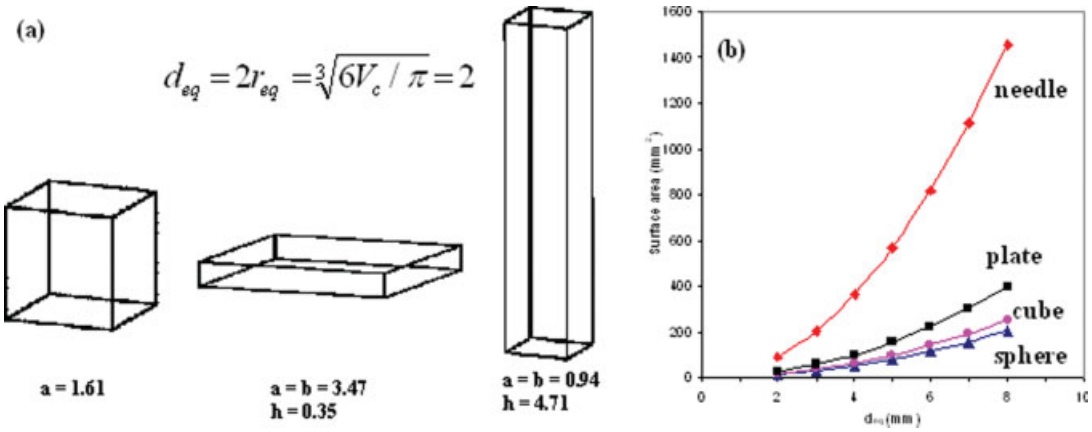

Figure 1. Variations of (a) crystal shape, and (b) the corresponding surface area with exactly same volume equivalent diameter (d_{eq}) of sphere.

[Color figure can be viewed in the online issue, which is available at www.interscience.wiley.com.]

crystal surface area such as crystal growth kinetics and rate, dissolution and absorption rates. Therefore, the monosized dimensional population balance (PB) models using volume equivalent parameters of spheres could lead to large errors when modeling crystallization processes of crystals that have needle-like or plate-like shape. Hence, this work has been motivated by the need to integrate morphology prediction, which has been restricted to individual crystals, with PB modeling which has not yet been effectively considered in terms of the effects of crystal shape.

Crystal morphology and its prediction

The morphology of a single crystal depends on the growth behavior of its different crystallographic faces.[8] Some faces grow very fast, and, thus, have little or no effect on the final crystal shape, while the ones that have most influence are the slow-growing faces. The growth of a given face is governed by both the crystal internal structure, such as packing arrangement of molecules and growth defects, and the external environmental conditions such as fluid shear, mechanical abrasion from vessels and impellers, heat and mass transfer, the physicochemical effects from interactions between crystal surfaces and the ambient phase (often a solution, and solvent or impurities).[9]

Early morphological modeling approaches were based on the geometrical Bravais-Freidel-Donnay-Harker (BFDH)[10] and energetic Hartman-Perdok[11] models, which account to different degrees for the effect of crystal internal structure on the morphology of a single crystal. The former uses the lattice geometry, such as cell dimensions and molecule positions, with the assumptions of the slowest faces being those with the highest density of material and the largest spacing between adjacent layers of material. The latter sets the growth rate of a crystal face to be proportional to the absolute value of the attachment energy[12] which is defined as the energy released on the addition of a growth slice to the surface of a growing crystal,[13,14] and is estimated using intermolecular interactions between a molecule on the face and the bulk of the crystal. These early methods have been widely used to predict the crystal shape of pharmaceutical crystals,[15–18] with some of them being implemented in commercial computer programs. The great advantage of the aforementioned approaches is that they are based on sound physical principles, with all that is required to implement these models is the internal structure information of the crystal, such as unit cell parameters, fractional atomic coordinates and symmetry information. However, they do not completely consider the effect of process operating conditions, such as reactor hydrodynamics and mother liquor environment which can impact upon the reliability of these methods, to correctly predict the morphology of the crystals for some processes.

A number of new approaches have also been developed over the past decade. These approaches use a modified attachment energy,[19,20] based on Hartman-Perdok theory, detailed kinetics principles[21–25] and Monte Carlo techniques[26,27] to include the effect of solvent, additives and supersaturation on the crystal shape into the morphological modeling. Roberts et al.[28] used a modified Hartman and Perdok's attachment energy to model the effect of solvent on morphology for the study of the molecular recognition at the crystal-solution interface. Similarly, Clydesdale et al.[19,20] modeled the crystal morphology in the presence of blocking and disruptive tailor-made additives. Detailed crystal growth kinetics was used in Bennema's group for the prediction of crystal morphology grown from solution.[23,29,30] In their method, the kinetic models are simplified to retain only one solvent dependent parameter, which can be derived from computer simulation of the solid-fluid interaction. A similar method was also developed in Doherty's group based on detailed crystal growth kinetics.[21,22,24,25] Their approach requires the calculation of the nature of the intermolecular interactions along the different growth directions, and has been used successfully to predict the shapes of a number of organic materials grown from solution.

Boerrigter et al.[26] used the Monte Carlo simulation technique to incorporate the effect of supersaturation on the crystal morphology. Their method can simulate crystal growth from an isotropic mother phase in any direction on any given crystal, and the dependence of the crystal morphology on supersaturation can be determined once information on the

relevant growth mechanism for the various faces is known. Recently, Gadewar and Doherty[31] developed a dynamic model for the prediction of the shape evolution of 2-D (two-dimensional) crystals from arbitrary initial shapes. The model can account for faces appearing and disappearing during the evolution, and also predict the crystal shape at steady-state. Zhang et al.[32] developed a model for the shape evolution of 3-D faceted single crystals, and applied this to two organic crystal systems: adipic acid and α-glycine grown from water. A number of comprehensive reviews on the background and applications of crystal morphological modeling can be found in literature.[9,33,34]

In summary, the whole evolution of research in the crystal shape modeling arena shows an optimistic future in the way to develop more realistic shape predictions. However, it is worth noting that almost all of the previous research has focused on the prediction of the shape of isolated single crystals, rather than on the broader behavior of a defined population of crystals within a typical reactor environment. Nevertheless, as will be discussed in more detail later, the prediction of morphology for a single crystal can provide an important based-line situation, such as the initial face locations, for subsequent morphological PB modeling.

Population balance modeling

A population balance (PB) model generally accounts for the convective processes that involve both the motion of particles in a system through their defined domains and their birth-and-death processes that can both terminate existing and produce new particles.[35,36] The PB modeling technique was developed a few decades ago, and has been used to model particulate processes including crystallization. Previous studies of industrial crystallization used monodimensional PB models.[42,43,44] Campos and Large[37] developed a numerical method to solve a transient PB equation using an Euler-Lagrange formulation, and tested the method against a few particulate systems with only one internal variable (particle mass), which is size-related and only one external coordinate. Iveson[45] presented a PB equation for modeling the wet granulation of a binary mixture of solids with four independent granule characteristic parameters: the granule solid-phase mass, the binder to solid mass ratio, the granule porosity, and the solid-phase mass fraction of one component. The use of the term multidimension needs some clarification, and it needs to be pointed out that the term of multidimension used previously in PB literature refers to only one size-related dimension, i.e., volume- equivalent spherical diameter, while other dimensions cited mostly represent other physical properties, such as particle location, porosity, and fraction ratio.

In an effort to incorporate crystal shape information into PB modeling, Puel et al.[46–48] developed a 2-D PB modeling approach to predict the growth of hydroquinone via representing the rod-like crystals of this material as rectangular parallelepipeds of length and width. In their method, the so-called method of classes was used to solve the nonlinear PB equations. The kinetic parameters for crystal nucleation and growth were estimated through the comparison between experimental and calculated data following the modeling strategy previously reported in literature.[49,50] The PB model demonstrated the ability to predict the time-variation of the crystal habit of the assumed rectangular parallelepipeds. Oullion et al.[51] carried out experiments of a plate-like organic material in a batch crystallization using *in situ* ATR FTIR spectroscopy for solute concentration estimation, and off-line image analysis to characterize discrete-time measurements of the 2-D crystal-size distributions. The 2-D PB model[46,47] was applied to the batch crystallization process for the kinetic modeling and identification, which included two secondary nucleation mechanisms and crystal growth mechanism in two directions.[52] Gerstlauer et al.[53–55] developed a PB model for the analysis and validation of continuous and batch crystallizers with detailed kinetic expressions for primary nucleation, crystal growth and attrition. The PB model itself involved one-size dimension though a second characteristic length of abraded crystal was introduced into the model through attrition function.[53,55] In their earlier work,[54] a second dimension was used to incorporate the crystal internal lattice strain into a PB model, and its effect was represented by different theories including deformation energies, mosaic spread and internal lattice strain. In a complementary study, Ma et al.[56] applied a 2-D PB modeling approach to simulate the growth of needle-like crystals of potassium dihydrogen phosphate with two characteristic length scales. A splitting method was employed to decompose the 2-D PB equation into a pair of 1-D equations, and each of them was then solved using a high-resolution descritization scheme via implementing a hybrid of the upwind scheme, and the Lax-Wendroff method through a flux limiter function, with the kinetic parameters being determined from experimental data. Briesen[57] used the same potassium dihydrogen phosphate system and the same kinetic parameters[56] to illustrate the numerical results of a reduced 2-D PB model. Coordinate transformation was performed to model the system by introducing two characteristic parameters: the crystal volume and a shape factor. Further model reduction was applied to form three coupled single PB equations using a predefined function for the 2-D crystal-size distribution. Recently, a new approach was developed by Zhang and Doherty[58] to combine a separate shape evolution model[31] with a standard 1-D PB model for the simultaneous prediction of crystal shape evolution and size distribution in solution crystallization processes. The method was applied to track both the crystal size and shape evolution of 2-D tablet-like succinic acid crystals, as grown from water, with fixed relative face growth rates being applied to all faces. Clearly, through using a reduced 2-D model for crystal systems which exhibit complex crystal morphologies, and, hence, with multiple facets is bound to lead to a loss of morphological information.

In this study, a morphological (or polyhedral) PB model is presented, which is able to incorporate more complicated crystal structures/shapes than needle-like crystals into PB modeling, therefore, can simulate the size-related dimensional evolution of crystals for each identified independent crystal face. In this new method, the initial facet structures can be obtained through either morphology prediction or using experimental studies of single crystals. The kinetic parameters for the crystal growth rates of each face can be estimated by experimental studies including single crystal investigations and batch crystallization using advanced techniques, such as specialized imaging and image analysis. From the predicted growth of different faces at different times during

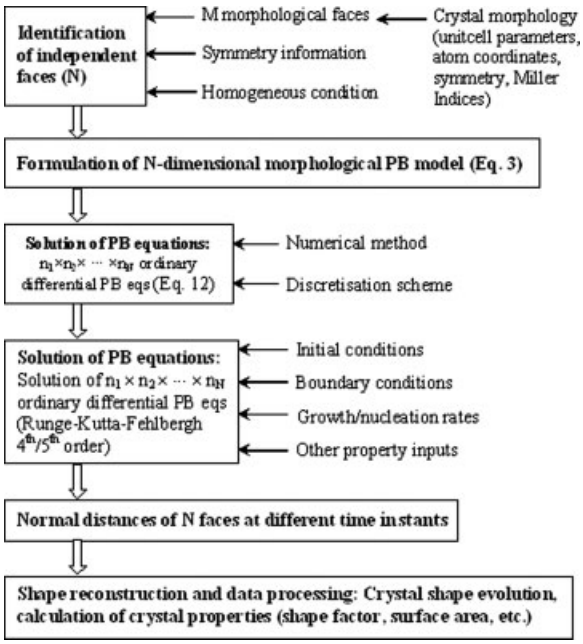

Figure 2. Morphological PB modeling methodology.

crystallization process, many important crystal properties, such as shape and growth rate can be evaluated and used for real-time monitoring, control and manipulation of crystal morphology. Potash alum ($KAl(SO_4)_2 \cdot 12H_2O$), a compound very well-studied in literature, is used as a representative material for case study in order to illustrate and validate the morphological PB modeling approach proposed.

Morphological Population Balance Modeling

Methodology

The overall scheme associated with the morphological (polyhedral) PB modeling methodology is illustrated in Figure 2. The method involves several steps including the identification of independent faces using the crystal morphology information, the formulation of a morphological multidimensional PB model, and the solution of the corresponding PB equation to predict the location variations for each independent crystal face, and the temporal reconstruction of crystal shapes during the crystallization process with post-processing enabling extraction of shape-related crystal properties including shape parameter, surface area and particle volume.

A crystal can be defined as a regular polyhedral solid bounded by plane faces, while the internal structure is composed of atoms or molecules arranged in a 3-D repeating structure. The 3-D arrangement of molecules can be represented by a crystal lattice, which illustrates how an atom or group of atoms (motif) associated with each point in the lattice is repeated in space. The repeating unit of the crystal lattice is often referred to as the unit cell with parameters, such as the vectors a, b and c along the crystallographic axes and the angles between them, α, β and γ. The internal crystal structure can be determined with the unit cell and the motif. The external structure of a crystal, crystal morphology, can be defined by the planes, the interfacial angles between the planes, and by using lattices directions. Any plane in a crystal can be described by the Miller Indices (hkl), such that the plane intercepts the crystallographic axes at the positions A′, B′ and C′ (Figure 3). For example, in a octahedral system as shown in Figure 3, the face (A′B′C′) has the Miller Indices of (111) calculated by $\frac{a}{OA'}, \frac{b}{OB'}$ and $\frac{c}{OC'}$. Similarly, the Miller Indices of other seven faces can be determined. The notation crystal form $\{hkl\}$ is used to describe the set of planes symmetrically equivalent to the plane (hkl). Therefore, in a cubic system ($a = b = c$, $\alpha = \beta = \gamma = 90^0$) the $\{111\}$ form can be shown to comprise eight symmetry-related faces, i.e., (111) $(11\bar{1})$, $(1\bar{1}1)$, $(\bar{1}11)$, $(1\bar{1}\bar{1})$, $(\bar{1}1\bar{1})$, $(\bar{1}\bar{1}1)$ and $(\bar{1}\bar{1}\bar{1})$.

Crystal structures can be solved through single crystal or powder X-ray diffraction studies, together with molecular modeling, which provide crystallographic information, such as unit cell parameters, atom coordinates, symmetry information and Miller Indices. With the known crystal structure of a compound, modeling software and experimental investigation can be used to study the crystal morphology and morphological changes. As shown in Figure 2, the morphological modeling software, HABIT95[3] and SHAPE,[7] can be used to provide detailed information of the crystal morphology including locations of all faces (normal distances from the faces to crystal center), and their corresponding corners with the input of crystallographic information from structure solution. The effect of additives, impurities and solvents on crystal morphology can also be predicted.[20,59] Single crystal experiments, such as X-ray topography[60] are also useful to investigate crystal morphology, defect, and to verify modeling results as well.

For a general PB concept, a PB model can be used to simulate the size distributions of crystal population with multidimensions, which may include multidimensional internal coordinates, such as size, temperature, composition, etc., multidimensional external coordinates referring to its physical locations, and the complicated processes, such as aggregation, breakage, nucleation, etc. in the reac-

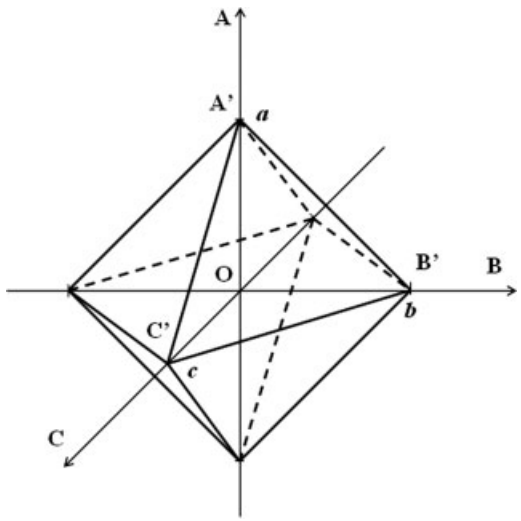

Figure 3. The eight morphological faces in an octahedral system: the Miller Indices of the face (A′B′C′) is (111), with other seven faces being symmetry-related to this face.

tor. However, in practice and under the power and capacity of the current computer systems, it is challenging to solve a general PB equation with such complication. Therefore, simplifications to highlight the importance of one variable or a group of variables have often been used to simulate the population variations in a reactor. With the symmetry information for all known crystal faces, the symmetry-related faces can be identified. Based on this, the total crystal faces can be classified into different face groups by their Miller Indices {hkl} primary form. By assuming homogeneous conditions surrounding a crystal, the growth behavior of the symmetry-related faces in each face group, can, thus, be regarded as being identical to each other. Therefore, each group of the symmetry-related faces can be considered as just a single independent face, hence, significantly reducing the number of the faces needed for the morphological PB model. If N groups of symmetry-related faces can be identified from the total of M faces considered, and the ith group (independent face) in the N groups has M_i number of symmetry-related faces, then the M faces obtained from morphological calculations or experimental studies could be reduced to N faces with $M = \sum_{i=1}^{N} M_i$ $(M_i \geq 1)$. Then an N-sized dimensional PB model can be developed to predict the morphological variations of the N faces during crystallization. For example, as shown in Figure 3, an octahedral system has a total of eight faces (M = 8) which are symmetry-related to each other. Under the earlier assumptions, the eight faces can be categorised into one group (N = 1) with $M_1 = 8$. Therefore, the octahedral system can be modeled with 1-D PB. With a proper solution method and necessary input conditions, such as initial and boundary conditions of the N faces, the growth rates of the N faces, etc. as shown in Figure 2, the N-dimensional morphological PB equations can be solved to predict the normal distance changes of the N faces at different times during crystallization in a reactor, i.e., under real operating conditions. Morphological modeling software can then be used to reconstruct the full crystal shape at individual times using the predicted normal distances of the N faces, which can be further processed for the calculations of many important crystal properties such as shape factor, surface area, volume, density etc., and their relationships with the operating conditions of a practical crystallization process. It is worth noting that if the homogeneous conditions, and/or symmetry of crystal shape cannot be applied to one face due to variations of hydrodynamics within a reactor, and/or addition of additives and impurities into the reactor for crystal shape manipulation, that face can be treated as an independent face, which therefore can be modeled as an additional independent dimension within the morphological PB model.

Formulation of morphological population balance equation

The mathematical formulation for multidimensional population balance has been discussed in literature, e.g., by Campos and Large.[37] Although in literature, the so-called multidimension is often interpreted as multiple-variables, i.e., a single-size dimension as volume equivalent spherical diameter plus other variables, such as particle location, porosity and fraction ratio, the same mathematical formulation can be extended to include multiple-size dimensions.

The mathematical formulation for multidimensional PB modeling, no matter employing a single-size dimension plus other variables, or multiple-size dimensions, can be given by Eq. 1

$$\frac{\partial \psi(\vec{x},\vec{y},t)}{\partial t} + \nabla \cdot [\psi(\vec{x},\vec{y},t)\vec{v}] + \sum_{i=1}^{N} \frac{\partial}{\partial x_i}[\psi(\vec{x},\vec{y},t)G_i(\vec{x},\vec{y},t)] = B(\vec{x},\vec{y},t) - D(\vec{x},\vec{y},t) + R(\vec{x},\vec{y},t) \quad (1)$$

where N is the number of internal variables for a crystal, $\vec{x}$ is the internal variable vector with N components, which can be parameters related to crystal size, shape, and physical properties, $\vec{y}$ is the external variable vector with the corresponding components of spatial coordinates (y_1, y_2, y_3), ψ is the number population density function of crystals in the internal variable range (x_i, $x_i + dx_i$, $i = 1,N$), and in the differential volume of $dy_1dy_2dy_3$, ∇ is the gradient operator for the $\vec{y}$ coordinates. The first term on the lefthand side of Eq. 1 is the accumulation term of population ψ. The second term donates to the convection of population ψ, in the $\vec{y}$ space with $\vec{v}$ being the velocity vector. The third term is the convection of population ψ, due to growth of particle in the $\vec{x}$ space with G_i being the growth rate. On the righthand side of Eq. 1, the first and second terms, $B(\vec{x},\vec{y},t)$ and $D(\vec{x},\vec{y},t)$, represent the birth and death terms of population ψ, due to all the processes during crystallization, such as aggregation, breakage, attrition, etc. (excluding nucleation), and the third term $R(\vec{x},\vec{y},t)$, is the nucleation term.

Theoretically, Eq. 1 can be solved for crystal population distribution with the proper initial and boundary conditions, and the combination of momentum, mass and heat transfer in the particulate system, in addition to the proper functions of aggregation, breakage, attrition, nucleation etc. processes in the reactor. However, the general multidimensional PB equation like Eq. 1 will form a set of multidimensional integrodifferential equations, due to the integration terms from the source terms, such as $B(\vec{x},\vec{y},t)$, $D(\vec{x},\vec{y},t)$, $R(\vec{x},\vec{y},t)$, and the solution of such complicated PB equations will be exceedingly difficult. In a well-mixed batch crystallizer, the influence of crystal positions in the crystallizer on population distributions can be ignored. In this study, a complex inorganic hydrate compound, potash alum, was specially chosen, which displays no known cleavage planes for particle fracture, while its strongly-bonded and equant particle morphology is not particularly known for extensive attrition behavior. The crystal surface chemistry for all three {111}, {100} and {110} of its crystal habit faces (see Figure 4) displays an intimate mixture of cation, anion and hydrating water molecules in such a manner that significant particle/particle agglomeration is not expected, and also not observed. Therefore, for this material it is reasonable to neglect the effect of agglomeration and breakage. However, generically the effect of agglomeration and breakage can be expected to be important sources of morphological change, and further development is definitely needed to incorporate such phenomena into the morphological PB model developed in this study. However, accepting the earlier assumptions for

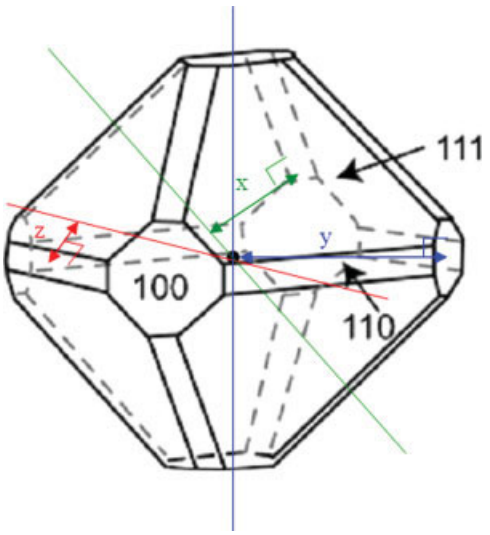

Figure 4. Morphology of potash alum crystal,[60] and of the three-size characteristic parameters (x, y, z) to be used in a morphological PB model for each independent crystal faces in a potash alum ($KAl(SO_4)_2{\cdot}12H_2O$) system.

[Color figure can be viewed in the online issue, which is available at www.interscience.wiley.com.]

the case of potash alum, a simplified version of Eq. 1 can be written as

$$\frac{1}{V_T(t)}\frac{\partial[\psi(\vec{x},t)V_T(t)]}{\partial t}+\sum_{i=1}^{N}\frac{\partial}{\partial x_i}[\psi(\vec{x},t)G_i(\vec{x},t)]=R(\vec{x},t) \quad (2)$$

It should be noted that, from now on, the $\vec{x}$ in Eq. 2 is an N-dimensional vector which will only represent the size-related parameters of a crystal in order to distinguish the multidimensional PB model presented here from the other PB models, which usually include only one size-related variable. Hence, in the following section, the case example of potash alum ($KAl(SO_4)_2{\cdot}12H_2O$) is presented to demonstrate and validate the morphological PB modeling technique.

Application of Morphological Population Balance Modeling to the Crystallization of Potash Alum from Solution

Single crystals of potash alum

Potassium (potash) alum, $KAl(SO_4)_2{\cdot}12H_2O$, crystallizes in the cubic structure with the space group $Pa\bar{3}$ with a = 12.158 Å and four molecules per unit cell. Morphology prediction and experimental studies[60–62] demonstrated that the morphology of potash alum is dominated by the octahedron {111}, the essentially smaller cube {100}, and rhomb-dodecahedron {110} (Figure 4). Three minor faces, {221}, {112} and {012}, can exist at early stages of crystallization, but they have been found to disappear quickly, hence, not normally seen in the normal morphology. These three primary growth forms are manifested in the external morphology through the multiplicities associated with cubic symmetry, which yields at total of twenty six crystal growth surfaces, i.e., eight {111}, six {100} and twelve {110} crystallographically-equivalent faces, respectively.

Single crystals of potassium (potash) alum, $KAl(SO_4)_2{\cdot}12H_2O$, can easily be grown from aqueous solution by evaporation or cooling from aqueous solution over the temperature range of 30–60°C.[60] The average relative growth rates (measured normal to the growth face) between the three main faces, {111}, {100}, {110} and three minor faces, {221}, {112}, {012}, at 30°C have been found to be roughly 1:5.3:4.8:9.5:11:27.[60] X-ray topographic studies,[61,62] examining crystal growth history and perfection, have been used to estimate the growth rates of three main faces at relative supersaturation levels of 0.0647 and 0.0678. Dispersion of the growth rates of {100} and {110} faces was observed in nearly all growth experiments, with the growth rate of the dominant {111} face being relatively stable.[60] This increase of growth rate may reflect the formation of a layer of small liquid inclusions on {100} surface, which marks the position and shape of face {100} at the moment of the disturbance of growth conditions.[60] After the formation of the inclusions, the growth rate of the face can be significantly increased, hence, resulting in smaller and smaller facet area leading to its disappearance. However, the fast growth of the {100} face has been found to slow down before it vanishes completely, leading in turn to a larger {100} face with the size of the face returning more or less to its former size. This decrease in growth rate could be caused by crystal growth defects, such as dislocations or strain, described by the mosaic structure of crystals, which has been investigated in literature (see Refs. 61–65). This aspect though is not considered here, as the purpose here is to develop and evaluate morphological PB modeling methodology. Therefore, the growth rate dispersion of both {100} and {110} faces has not been included in these calculations. However, further investigation is underway to incorporate this more complex behavior into the morphological PB modeling method.

Morphological population balance equation for potash alum

Reflecting the potash alum crystal having a total of 26 habit faces (M = 26), a geometric center can be found (Figure 4). The normal distance from a crystal face to the geometric center will form one-dimension for the morphological PB model. While, in theory, a morphological PB model with 26 dimensions is needed, since some faces, such as the 8 {111} faces (M_1 = 8), are symmetry-related and supposed to have the same surrounding growth environment, hence, same growth rates, these faces can be modeled as one-dimension (x) in the PB model. Similarly, the 6 {100} faces (M_2 = 6) and 12 {110} faces (M_3 = 12) will form the second y, and third z dimensions, respectively, in the model. Therefore, the total number of independent faces identified is 3 (N = 3). It is reasonable to assume that both the smallest crystal grown from nucleation, which, in PB calculation, is the smallest size group, and the final product have the same number of crystal faces, i.e., the similar crystal shape. Therefore, the total dimensions of the formed morphological PB equation equal to the total number of identified independent

faces. For the potash alum system, a 3-D morphological PB model, the corresponding three parameters, x, y, z, shown in Figure 4, can be formed to model its morphological changes when growing from aqueous solution. It should be noted that it is not necessary for the x, y, z parameters to be perpendicular to each other, as they are only normal distances from three faces to the crystal center. Also in this study and for simplicity, the effect of both primary and secondary nucleation of potash alum on population distributions was not considered. Accepting these assumptions the morphological PB equation of Eq. 2, can, thus, be written as follows

$$\frac{1}{V_T(t)}\frac{\partial}{\partial t}[\psi(x,y,z,t)V_T(t)] + \frac{\partial}{\partial x}[G_1(x,t)\psi(x,y,z,t)] + \frac{\partial}{\partial y}[G_2(y,t)\psi(x,y,z,t)] + \frac{\partial}{\partial z}[G_3(z,t)\psi(x,y,z,t)] = 0 \quad (3)$$

The first term on the lefthand side is the accumulation term of population. The second, third and fourth terms are the population changes for the three main habit faces, respectively, due to crystal growth in the corresponding directions. It is worth noting that Eqs. 2 and 3 represent generic formulations and so can incorporate more sophisticated situations, e.g., growth rate models defined as a function of crystal size in addition to supersaturation.

Crystal growth rates of individual faces

Nollet et al.[66] measured the solubility of potash alum, and compared the experimental results with those obtained by Mullin,[8] Synowietz and Schafer,[67] and Barrett and Glennon.[68] The following solubility equation[66,68] was used in this study

$$\ln(C^*) = 12.1/T + 10.47\ln(T) - 65.73 \quad (4)$$

The growth rate of a single potash alum crystal at a constant solution temperature was measured by Matsuoka et al.[69,70] The corresponding relative supersaturation σ, of the solution had a constant value of 0.022. The growth rate of the {111} face was also measured by Mullin and Garside.[71] These correlated growth rates of this face as a function of the relative supersaturation are listed below:
Matsuoka et al.[69]

$$G_1 = 4.62 \times 10^{-6}\sigma^{1.6} \quad \text{at } 298K \quad (5)$$

Matsuoka et al.[70]

$$G_1 = 6.00 \times 10^{-6}\sigma^{1.6} \quad \text{at } 303.15K \quad (6)$$

Mullin and Garside[71]

$$G_1 = 7.52 \times 10^{-6}\sigma^{1.6} \quad \text{at } 305.15K \quad (7)$$

where σ is the relative supersaturation calculated by $C/C^* - 1$ with C, the solute concentration, being defined as the molar weight per volume of solution in a reactor. However, there was no such correlations available for other two main habit faces, {100} and {110}, probably due to the difficulties of distinguishing these smaller faces by the CCD or TV cameras used in the experiments.

A series of polycrystal growth experiments at different flow velocities and relative supersaturation levels was carried out by Nollet et al.[66] to investigate the face growth rates of potash alum crystal using a reaction flow cell with crystal seeds fixed at the bottom of the cell. The measured growth rate of the {111} face was found to be more uniform over time than the other faces, but a wide variation in growth rates between the different faces was observed for all experiments, which could be caused by a combination of the face index, the face size and the flow direction with respect to the face orientation. Hilgers and Urai[72] obtained an overall growth rate equation of potash alum crystals as a function of relative supersaturation and flow velocity by fitting the crystal growth data from Garside[73]

$$G_{overall} = (6.5 + 13\,v^{0.3})6.0 \times 10^{-8}\sigma^{1.5} \quad (8)$$

The crystal growth rates of the {111} and non-{111} faces from Ristic et al.[62], Nollet et al.[66] and the calculated growth rate of the {111} face by Eqs. 5–7, and also the overall growth rate with different flow velocities from Eq. 8 are given in Figure 5. From this, it can be seen that the calculated overall growth rates using Eq. 8 with a flow velocity of 0.05m/s, are comparable to those rates of the {111} face from Ristic et al.[62] and Nollet et al.[66], particularly in the relative supersaturation range of 0.07–0.11, while the Eqs. 5–7 from Matsuoka et al.[69,70] and Mullin and Garside[71] produced about 10 times higher growth rates of the {111} face. Therefore, in this study, the equation (Eq. 8) from Nollet et al.[66] with flow velocity of 0.05 m/s, was used to calculate the growth rates of the {111} face

$$G_1 = 7.753 \times 10^{-7}\sigma^{1.5} \quad (9)$$

The growth rates of the {100} and {110} faces can be estimated according to the ratio of growth rate between the {100}, {110} faces and the {111} face. The relative growth rates between the {111}, {100} and {110} faces at two rela-

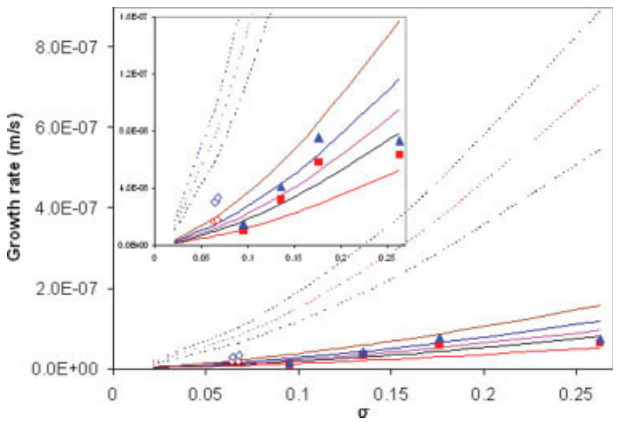

Figure 5. Growth rate of potash alum crystals (○ and △ — {111} and non-{111} faces;[61] ▲ and ■ — {111} and non-{111} faces;[66] solid lines — overall growth rates calculated with Eq. 8 at different flow velocities of 0.0, 0.01, 0.05, 0.2, 1.0m/s; dashed lines — growth rates of the {111} face obtained with Eqs. 5–7).

[Color figure can be viewed in the online issue, which is available at www.interscience.wiley.com.]

tive supersaturation levels (0.0647 and 0.0678) obtained by Ristic et al.[62] are 1:2.2:1.4 and 1:2.3:1.5, respectively. The average relative growth rates between the {111} and non-{111} faces from the experimental data of Nollet et al.[66] are 1:1.4 at relative supersaturation of 0.095 and 1:1.3 at relative supersaturation of 0.176, which is comparable to the results from Ristic et al.[62] In this study, the average relative growth rates between the {111}, {100} and {110} faces from Ristic et al.,[62], i.e., 1:2.25:1.45, were used to calculate the crystal growth rates of the {100} and {110} faces

$$G_2 = 1.744 \times 10^{-6}\sigma^{1.5} \tag{10}$$

$$G_3 = 1.124 \times 10^{-6}\sigma^{1.5} \tag{11}$$

It is worth noting that the ratios of face growth rates are not necessarily required to be constant in this method. The growth rates of individual faces can vary independently, and be obtained via techniques, such as imaging and image analysis.[74–76] The growth rates of individual faces, {111}, {100} and {110}, as shown in Eqs. 9–11 have similar exponents albeit with differing proportionality constants for this study. It is not explicitly known what the interface kinetic mechanism is, i.e., the BCF[77] or birth-and-spread,[78] but X-ray topographic examination has revealed the presence and impact of screw-component dislocation on growth. In addition, growth rate dispersion, particularly on {100} face has also been observed.[60] However, the morphological PB modeling methodology developed in this study can incorporate more complicated growth rate functions, e.g., models that are dependent on crystal size in addition to supersaturation.

Numerical solution of the morphological population balance equation

The discretization method, moment of classes, was used to solve the 3-D morphological PB equation by extending the numerical solution procedure for a 2-D PB equation described in.[38,46] The 3-D size domain was discretized into n_1, n_2, n_3 classes, i.e., CL_i ($i = 1, n_1$), CL_j ($j = 1, n_2$), CL_k ($k = 1, n_3$). The corresponding size and characteristic dimensional length of each class in each dimension are $\Delta x_i = x_i - x_{i-1}$, $\Delta y_j = y_j - y_{j-1}$, $\Delta z_k = z_k - z_{k-1}$ and $\bar{x}_i = (x_{i-1} + x_i)/2$, $\bar{y}_j = (y_{j-1} + y_j)/2$, $\bar{z}_k = (z_{k-1} + z_k)/2$, respectively. Therefore, a system of $n_1 \times n_2 \times n_3$ 3-D classes was formed, with the class $Cl_{i,j,k}$, being delimited by (x_i, x_{i-1}), (y_j, y_{j-1}), (z_k, z_{k-1}). By integrating Eq. 3 over class $Cl_{i,j,k}$ of x, y and z, a set of $n_1 \times n_2 \times n_3$ ordinary differential equations can be formed as follows

$$\frac{1}{V_T(t)}\frac{d}{dt}[N_{i,j,k}(t)V_T(t)] + [FX^O_{i,j,k}(t) - FX^I_{i,j,k}(t)] + [FY^O_{i,j,k}(t) - FY^I_{i,j,k}(t)] + [FZ^O_{i,j,k}(t) - FZ^I_{i,j,k}(t)] = 0 \tag{12}$$

where $N_{i,j,k}(t)$ is the number of crystals in the class $Cl_{i,j,k}$

$$N_{i,j,k}(t) = \int_{x_{i-1}}^{x_i}\int_{y_{j-1}}^{y_j}\int_{z_{k-1}}^{z_k}\psi(x,y,z,t)dxdydz \tag{13}$$

and the first term on the lefthand side of Eq. 12 is the accumulation term, and can be rewritten as

$$\frac{1}{V_T(t)}\frac{d}{dt}[N_{i,j,k}(t)V_T(t)] = \frac{N_{i,j,k}(t)}{V_T(t)}\frac{dV_T(t)}{dt} + \frac{N_{i,j,k}(t+1) - N_{i,j,k}(t)}{\Delta t} \tag{14}$$

and the second, third and fourth terms on the lefthand side of Eq. 12 are the net flows of crystals in class $Cl_{i,j,k}$ due to crystal growth with the superscripts O and I, denoting the crystal flowing outletting from and inletting into the $Cl_{i,j,k}$ class

$$FX^O_{i,j,k}(t) - FX^I_{i,j,k}(t) = \int_{x_{i-1}}^{x_i}\int_{y_{j-1}}^{y_j}\int_{z_{k-1}}^{z_k}\frac{\partial}{\partial x}[G_1(x,t)\psi(x,y,z,t)]dx\,dy\,dz \tag{15}$$

$$FY^O_{i,j,k}(t) - FY^I_{i,j,k}(t) = \int_{x_{i-1}}^{x_i}\int_{y_{j-1}}^{y_j}\int_{z_{k-1}}^{z_k}\frac{\partial}{\partial y}[G_2(y,t)\psi(x,y,z,t)]dx\,dy\,dz \tag{16}$$

$$FZ^O_{i,j,k}(t) - FZ^I_{i,j,k}(t) = \int_{x_{i-1}}^{x_i}\int_{y_{j-1}}^{y_j}\int_{z_{k-1}}^{z_k}\frac{\partial}{\partial z}[G_3(z,t)\psi(x,y,z,t)]dx\,dy\,dz \tag{17}$$

The crystal flow fluxes in x direction (Eq. 15) can be calculated using the following formulation and similar formulation can be obtained for the other two directions

$$FX^I_{i,j,k} = G_1(\bar{x}_{i-1},t)\left[a_{i-1}N_{i-1,j,k}(t) + b_{i-1}N_{i,j,k}(t)\right] \tag{18}$$

$$FX^O_{i,j,k} = G_1(\bar{x}_i,t)\left[a_iN_{i,j,k}(t) + b_iN_{i+1,j,k}(t)\right] \tag{19}$$

where $a_i = \Delta x_{i+1}/[\Delta x_i(\Delta x_{i+1} + \Delta x_i)]$ and $b_i = \Delta x_i/[\Delta x_{i+1}(\Delta x_{i+1} + \Delta x_i)]$ with boundary conditions for crystal flow fluxes as

$$FX^I_{1,j,k}(t) = FY^I_{i,1,k}(t) = FZ^I_{i,j,1}(t) = 0 \tag{20}$$

$$FX^O_{1,j,k}(t) = FY^O_{i,1,k}(t) = FZ^O_{i,j,1}(t) = 0 \tag{21}$$

The solid concentration $C_S(t)$, in unit volume of suspension in a well-mixed batch crystallizer for a given time t, can be calculated by

$$C_S(t) = \frac{\rho_s}{M_s}\int_x\int_y\int_z V_c \cdot \psi(x,y,z,t)dx\,dy\,dz \tag{22}$$

whereas, with negligible effect of crystallization and temperature variation on the total volume, the volume of suspension $V_T(t)$, can be calculated by $V(0)/[1-M_s/\rho_sC_s(t)]$, and the solute concentration C(t), can be estimated with $C(0) - C_S(t)/[1-M_s/\rho_sC_s(t)]$.

The discretized population balance equations (Eq. 12), together with a Gaussian-type initial population distribution, and the boundary conditions (Eqs. 20 and 21), were solved in the crystal size ranges of 0–43.2 μm, 0–64 μm and 0–60 μm in x, y and z directions, respectively, with the number of the size classes being $118 \times 116 \times 116$ and the correspond-

ing width being 0.36 × 0.55 × 0.52 μm. The 1.58 × 10^6 discretized population balance equations generated in ordinary differential form were solved simultaneously using the Runge-Kutta-Fehlbergh 4th/5th-order solver[79] with automatic time-step control, and the criteria of the absolute and relative tolerance being 10^{-6} and 10^{-4}, respectively. Test runs with either larger number of size classes and smaller corresponding width, or smaller absolute and relative tolerance produced similar prediction. The 3-D population balance distributions were obtained via solving the corresponding equations with a desktop Dell PC (Pentium 4 2.4GHz processor and 1.0Gb Ram) running Microsoft Windows XP operating system, with typical computing time being about 20 min. However, it is worth noting that there is scope for further research in this direction to develop more effective solution methods, in particular when the approach is further developed to consider the effects of agglomeration, breakage, secondary nucleation etc. The use of higher resolution discretization schemes, and/or employment of other solution methods, such as method of lines[54] or a generalized finite-element scheme[53] or moving grid technique[80] with modifications, or a hierarchical solution strategy, based on a multilevel discretization[81] offers promise in this respect.

Real-time reconstruction of crystal shape

By solving the morphological PB equation for a time interval of Δt, the growth of individual faces, {111}, {100} and {110}, can be obtained, and, hence, used to calculate the new locations of the corresponding crystal faces, with respect to their previous locations. In this the updated normal distances for the individual faces, together with their corresponding face orientation, can be used to form a set of linear equations with the solutions of these equations generating the coordinates of all the corners of the crystal. For some simple shaped crystals, the geometric relationship between the corner coordinates and the normal distance and face orientation can be established through pure mathematical manipulation. With the help of visualisation software, such as Cerius[2,1], the new crystal shape following crystallization process for a time interval of Δt can be displayed and, subsequently, used to estimate the resultant crystal properties, such as shape distribution, mean-size distribution, area changes of individual faces etc. For the potash alum crystal system with its three main habit faces (Figure 4), the Cartesian coordinates of all the corners of the crystal can be calculated using a set of mathematical formulas after complicated geometric operations and manipulations. As shown in Figure 4, for this system there are 48 corners which are related to each other through geometric symmetry. The Cartesian coordinates (x_1^*, y_1^*, z_1^*) of one typical corner can be calculated by

$$x_1^* = \sqrt{2}z - y \tag{23}$$

$$y_1^* = \frac{\sqrt{6}}{2}x - z \tag{24}$$

$$z_1^* = y \tag{25}$$

The coordinates of the other 47 corners are determined by any interchange of x_1^*, y_1^* and z_1^*, or any sign change of one of the x_1^*, y_1^* and z_1^*, for example, (z_1^*, y_1^*, x_1^*), or ($-x_1^*$, y_1^*, z_1^*). The volume of a potash alum crystal can be calculated by

$$V_c = 4\left[\sqrt{3}x^3 - (\sqrt{3}x - y)^3 - 3\left(\frac{\sqrt{6}}{2}x - z\right)^2(2\sqrt{2}y - \sqrt{6}x) - 4\left(\frac{\sqrt{6}}{2}x - z\right)^3\right] \tag{26}$$

and the corresponding spherical equivalent diameter d_{eq}, and radius r_{eq}, associated with the polyhedral crystal is obtained as follows:

$$d_{eq} = 2r_{eq} = \sqrt[3]{6V_c/\pi} \tag{27}$$

The areas of {111}, {100} and {110} habit can be obtained by

$$A_{\{111\}} = 24\left\{\frac{\sqrt{3}}{2}x^2 - \left[\frac{\sqrt{3}}{2}(\Delta a)^2 + 2\sqrt{3}x\Delta b - 4\Delta a\Delta b + \sqrt{2}(\Delta b)^2\right]\right\} \tag{28}$$

$$A_{\{100\}} = 12[(\Delta a)^2 - 4(\Delta b)^2] \tag{29}$$

$$A_{\{110\}} = 24\Delta b(2\Delta b + \sqrt{6}x - 2\sqrt{2}\Delta a) \tag{30}$$

where $\Delta a = \sqrt{3}x - y$ and $\Delta b = \sqrt{6}/2x - z$.

Results and Discussions

Population distributions of individual faces

Figure 6 shows the population distributions of individual faces at different time instants. It can be seen that the shape of population distributions is kept being Gaussian-type, and both the peak values of the population and their full width at half maximum (FWHM) are almost kept unchanged during crystallization process. The starting normal distances to the faces {111}, {100} and {110} have been set to about 10 μm, i.e., more spherical shaped crystals i.e., representative of the crystals at a size close to their initial nuclei formulation. According to the Gibbs/Wulff theory,[82] the spherical shaped crystals used for the simulation reflect the shape of nuclei generated, because less free energy is required. In addition, a transformation of 3-D growth to 2-D surface growth may happen at an early stage (small size range) of crystal growth. After crystallization has elapsed 1,000 s, the normal distance to the {111} face from the geometric center of the crystal has been doubled. However, the normal distance to the {100} face has changed from about 10 μm to around 40 μm, i.e., about four times. These results are directly related to the crystal growth rates of individual faces employed in the simulation. It is worth noting that the Gaussian-type distribution of crystal population for each face was indirectly confirmed by the crystal-size distribution of potash alum obtained in a batch crystallizer.[83]

By fixing two characteristic parameters of the morphological PB model at their corresponding mean values, the population distributions of the third parameter at different crystallization times (500, 700, 900, 1,100, 1,300 and 1,500 s) are plotted in Figure 7. It was found that the initial Gaussian distributions of population were preserved well with the curve-

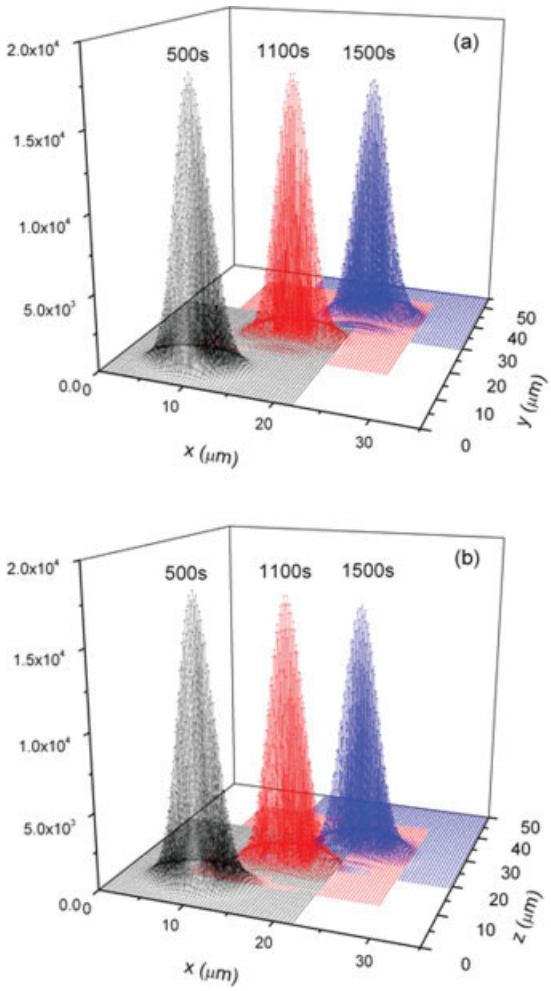

Figure 6. 2-D population distributions at crystallization times of 500 (black), 1,100 (red), and 1,500 (blue) seconds, with (a) {110} face located at its corresponding mean values, and (b) {100} face located at its corresponding mean values.

[Color figure can be viewed in the online issue, which is available at www.interscience.wiley.com.]

fitting parameter R^2, being over 0.99. During crystallization process, the maximum numbers of crystals in the class for the corresponding mean values were slightly decreased from 1.81×10^4 at 500 s to 1.64×10^4 at 1500 s. The corresponding FWHM values were increased from 4 μm at 500 s to 4.02 μm at 1,500 s for the {111} face, 4.38 μm for the {100} face, and 4.12 μm for the {110} face.

Crystal growth of individual faces

Figure 8 shows the crystal growth rate variations of three different faces of potash alum during the crystallization process. The growth rate r_{eq}, based on a volume equivalent spherical radius using the simulated crystal growth of each face is also plotted in Figure 8 for comparison. It can be seen that the growth rates of three different faces, {111}, {110} and {100}, have been predicted by the morphological PB model with good agreement with the data from literature. Some variations can be found in Figure 8 due to the implementation of the numerical method, notably, the adopted mesh size. Clearly smallest mesh sizes should be chosen, as long as the computational times are acceptable, and future

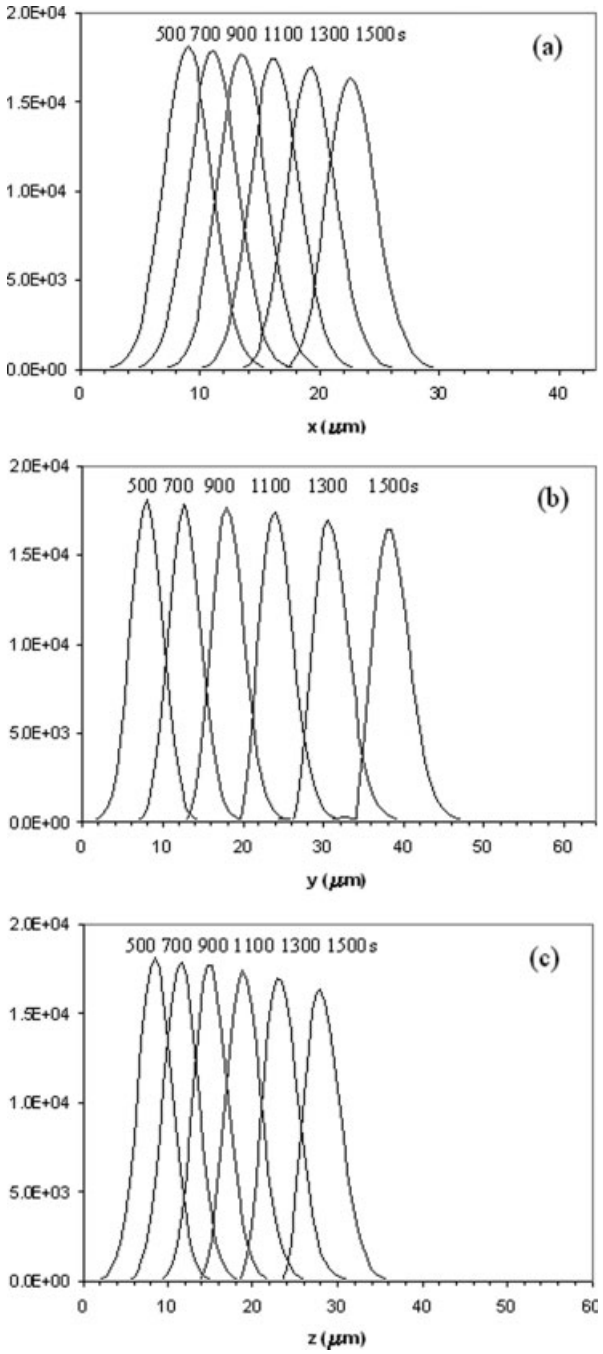

Figure 7. Population distributions of individual faces during crystallization with (a) {100} and {110} faces located at their corresponding mean values; (b) {111} and {110} faces located at their corresponding mean values; and (c) {111} and {100} faces located at their corresponding mean values.

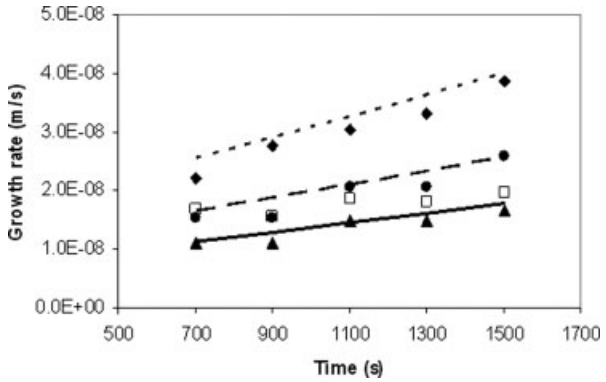

Figure 8. Crystal growth rates of three individual faces for potash alum (▲, ◆ and ● — simulation using the morphological PB model for {111}, {100} and {110} faces, respectively; solid line, dotted line and dashed line — calculation using Eqs. 9–11, respectively; □ — growth rate, based on volume equivalent radius r_{eq}).

research is also clearly needed in order to develop more effective methods for solving morphological PB equations, in particular, when the effects of agglomeration, breakage, secondary nucleation, and so on, need to be included in the equations. The equivalent growth rate r_{eq}, is close to that of face {111}, which is the dominant face with the slowest growth rate. The corresponding variations of the normal distance from each face with respect to the geometric center during the crystallization process are shown in Figure 9. At the starting time (500 s), three faces have similar perpendicular distances from the crystal geometric center. However, after 1,000 s, the normal distances of faces {100} and {110} are over two and 1.5 times, respectively, longer than that for face {111}. The equivalent radius of potash alum (Figure 9) is close to the normal distance of face {110}.

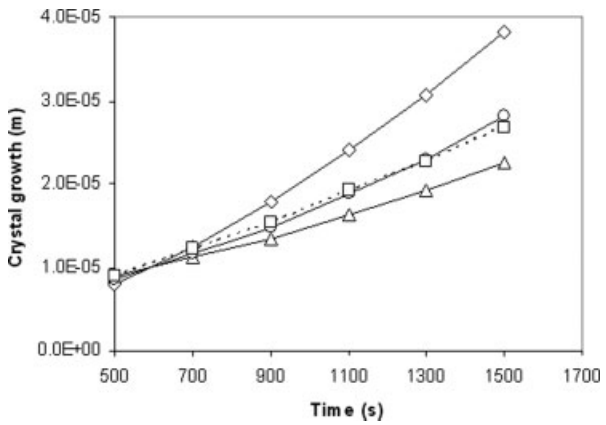

Figure 9. Growth of three faces against crystallization time (solid line with open triangles — {111} face; solid line with open diamonds — {100} face; solid line with open circles — {110} face; dashed line with open square — volume equivalent radius calculated with Eq. 27).

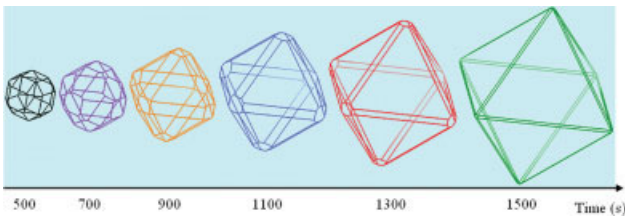

Figure 10. Crystal shape evolution during crystallization process of potash alum.

[Color figure can be viewed in the online issue, which is available at www.interscience.wiley.com.]

Shape predictions at different times

Figure 10 shows the crystal shape evolution with time for potash alum knowing that the {100} and {110} faces will eventually disappear with the crystal expected to exhibit pure octahedral diamond-like morphology at steady state under the current simulation conditions. Such pure octahedral shaped crystals have been observed for potash alum by Amara et al.[83] following seeded crystallization with a relative supersaturation of 0.1, and constant solution temperature of 32°C. A more quantitative comparison between modeling, and these data is not possible due to the different operating conditions. In addition, some caution is needed in terms of direct comparison, mindful that growth rate dispersion (GRD) may play a role particularly on the faster growing {100} faces, since GRD tends to cause such faces to have a reduced growth rate, particularly for larger crystals (~cm) when the surface areas of these faces become relatively small. In experimental observations on larger crystals rarely reveal a pure {111} morphology. In other words, growth rate dispersion could have prevented the disappearance of the {100} faces. The fundamental reasons for this are not clear, but presumably they are related to the development of strain within the {100} growth sector, enhanced through the approach of strained growth sector boundaries between the {100} and {111} surfaces, which becomes enhanced when the surface area is small, i.e., there is clear separation of growth sector boundaries.[60] Observation on micro crystals in contrast tends to reveal the pure {111} morphology, suggesting a possible size-dependent origin for the observed growth rate dispersion. Another factor that can possibly affect crystal shape evolution is attrition, through damaging the corners of a {111} octahedron and subsequently regrowing the {100} faces. Therefore, future research on the morphological population balance model should investigate the influence of attrition, as well as growth rate dispersion. Comparing Figures 4 and 9, the crystal shapes at times of 1,100 s and 1,300 s are very close to the morphology of potash alum crystal obtained from single crystal study.[60] Figure 11 indicated that the areas of faces {100} and {110} are reduced to very small values with increasing crystallization time, while the area of the dominated face {111} has increased dramatically. The total surface areas of the potash alum crystals broken down from the sum of the surface areas of {111}, {100} and {110} faces, together with the spherical areas with the corresponding equivalent radii (r_{eq}) during crystallization process are also given in Figure 11. It can be seen that the surface areas of potash alum crystal, based on the simulated results of the

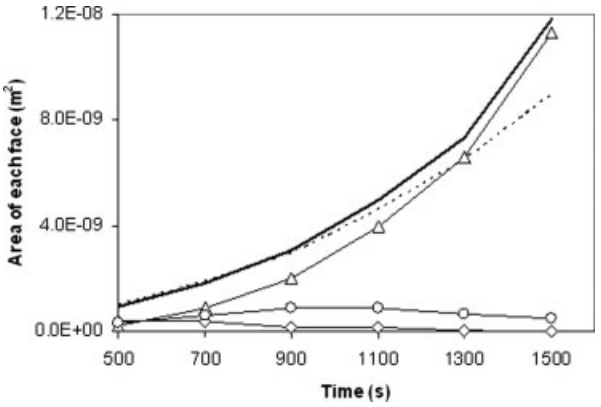

Figure 11. Area variations of three individual faces calculated using Eqs. 28–30 (solid line with open triangles — {111} face; solid line with open diamonds — {100} face; solid line with open circles — {110} face; solid line — {111} + {100} + {110} faces; dotted line — volume equivalent sphere with r_{eq}).

morphological PB model were larger than the ones with the equivalent diameter of sphere at later stages of crystallization. As surface area is one of the very important properties for crystallization process, downstream processing, and also the final product performance, the difference of surface areas presented here indicates the necessity of using the morphological PB model to capture important crystal properties when the crystal shape cannot realistically be modeled on a sphere-like one.

In single crystal studies,[60,61] dispersion of crystal growth rate of faces {100} and {110} was observed in several experimental studies. Ristic et al.[61] suggested that the growth rate variation of these faces might be caused by a high-degree of lattice strain. A model for this would be considered with the growth sector boundaries approaching each other causing the strain to be built-up to a point where the total strain developed per unit volume in the sector would be sufficient to make the free energy difference between the starting phase and crystal, the driving force for crystallization, negligibly small, i.e., the effective solubility for the effected {100} face is increased, lowering supersaturation, and reducing the growth rate to a point, where growth might stop all together. At higher supersaturation, the strain effect is overcome and growth can again continue.[61] From the simulation results of this study, the areas of faces {100} and {110} at time of 1,500 s become very small (see Figures 10 and 11), and eventually completely disappeared. Therefore, in such a case the morphological PB with three-dimensions becomes a 1-D PB model. In single crystal studies as discussed previously, the growth rates of faces {100} and {110} will slow down due to the high-level of crystal strain, giving rise to the onset of growth rate dispersion.

Concluding Remarks

Crystals, particularly organic crystals of speciality chemicals, such as pharmaceuticals grown from solution can produce materials with specific crystal shape and size distributions, which can have important impact on the end-use performance of the product and downstream processing. Traditionally, crystallization population balance modeling has been conducted mainly using a monodimension spherical equivalent model without considering the effect of crystal morphology. A few recent attempts in literature to consider crystal shape have been restricted to two-dimensions only. In this study, a methodology to predict the variations of individual crystal faces during crystallization has been developed by integrating crystal morphology into morphological population balance modeling with multiple-size dimensions. The methodology was introduced by reference to potash alum with the simulation results being qualitatively validated by literature data.

Acknowledgments

The work presented in this article is funded by the UK Engineering and Physical Sciences Research Council (EPSRC) (Grant references: EP/C009541/1 and EP/E045707/1). We would like to thank the support for the projects from the industrial collaborators, including Dr Richard J. Tweedie, Mr Andy Prior and Mr Duncan Roberts of Malvern Instruments, Ltd., Dr Ivan Marziano and Professor Robert Docherty of Pfizer Global Res & Dev, Dr Gerry Steele of AstraZeneca R&D, Dr Dominic Rhodes and Dr Mike J. Quayle of Nexia Solutions, Ltd., Dr Neil George of Syngenta and Dr Chris Blatchford of 3M Health Care. The authors would also like to thank Malvern Instruments for supporting the University of Leeds – Malvern Partnership: IntelliSense (www.intellisense.org.uk/).

Notation

A, B, C = crystallographic axes
A', B', C' = positions that a plane intercepts with the crystallographic axes
$A_{\{111\}}, A_{\{100\}}, A_{\{110\}}$ = surface area of {111}, {100} and {110} faces, m^2
a, b, c = unitcell vector, Å
a_i, b_i = coefficient, m^{-1}
$B(\vec{x}, \vec{y}, t)$ = birth term of crystal, [nb] m^{-3} m^{-3} s^{-1}
C = solute concentration, mol m^{-3}
C^* = solubility, mol m^{-3}
CL_i, CL_j, CL_k = monodimensional class in x, y and z directions
$Cl_{i,j,k}$ = 3-D class
C_S = concentration of solid in the suspension, mol m^{-3}
$D(\vec{x}, \vec{y}, t)$ = death term of crystal, [nb] m^{-3} m^{-3} s^{-1}
dy_1, dy_2, dy_3 = differential distances in y_1, y_2, y_3 directions, m
d_{eq} = equivalent diameter, m
$FX_{i,j,k}, FY_{i,j,k}, FZ_{i,j,k}$ = net flow rate of crystals in class $Cl_{i,j,k}$ in x, y and z directions, [nb] m^{-3} s^{-1}
G_i $(i=1,N)$ = crystal growth rate in i direction, m s^{-1}
G_1, G_2, G_3 = growth rate in x, y and z direction, m s^{-1}
$G_{overall}$ = overall crystal growth rate, m s^{-1}
M = total number of habit faces of a crystal
M_i $(i=1,N)$ = number of symmetry-related habit faces
M_s = molecular weight of solid, kg mol^{-1}
N = number of independent habit faces
$N_{i,j,k}$ = number of crystals in the class $CL_{i,j,k}$, [nb] m^{-3}
n_1, n_2, n_3 = number of classes in x, y and z directions
$R(\vec{x}, \vec{y}, t)$ = nucleation term, [nb] m^{-3} m^{-3} s^{-1}
t = time, s
T = solution temperature, K
V_c = volume of crystal, m^3
V_T = total volume of suspension, m^3
$\vec{v}$ = velocity vector, m s^{-1}
v = flow velocity, m s^{-1}
$\vec{x}$ = internal variable vector

x, y, z = characteristic parameters of crystal, m
x_1^*, y_1^*, z_1^*, = Cartesian coordinate of one typical corner, m
x_i, y_j, z_k = discretized characteristic parameters of crystal, m
$\bar{x}_i, \bar{y}_j, \bar{z}_k$ =characteristic parameters of class CL_i, CL_j and CL_k, m
$\vec{y}$ = external variable vector
y_1, y_2, y_3 = spatial coordinates, m

Greek letters

α, β, γ = unitcell angles, °
$\Delta x_i, \Delta y_j, \Delta z_k$ = extent of classes CL_i, CL_j and CL_k, m
ρ_s = density of solid, kg m^{-3}
ψ = number population density function in the suspension, [nb] m^{-3} m^{-3}
σ = relative supersaturation (= $C/C^* - 1$)

Literature Cited

1. Accelrys. http://www.accelrys.com/cerius2/.
2. Clydesdale G, Roberts, KJ, Docherty, R. HABIT - a program for predicting the morphology of molecular crystals. *Comp Phys Comm*. 1991;64:311–328.
3. Clydesdale G, Roberts KJ, Docherty R. HABIT95 - A program for predicting the morphology of molecular crystals as a function of the growth environment. *J of Crystal Growth*. 1996;166:78–83.
4. Clydesdale G, Roberts, KJ, Docherty R. HABIT95, Quantum Chemistry Program Exchange. Program no. 670, Bloomington, IN; 1996.
5. Docherty R, Roberts KJ, Dowty E. Morang - a computer-program designed to aid in the determinations of crystal morphology. *Comp Phys Comm*. 1988;51:423–430.
6. Hammond RB, Pencheva K, Roberts KJ. A structural-kinetic approach to model face-specific solution/crystal surface energy associated with the crystallization of acetyl salicylic acid from supersaturated aqueous/ethanol solution. *Crystal Growth & Design*. 2006;6: 1324–1334.
7. SHAPE for windows 7.1. www.shapesoftware.com. 2006.
8. Mullin JW. *Crystallization*. 4th ed. USA: Butterworth-Heinemann; 2001.
9. Winn D, Doherty MF. Modeling crystal shapes of organic materials grown from solution. *AIChE J*. 2000;46:1348–1367.
10. Donnay J, Harker D. A new law of crystal morphology extending the Law of Bravais. *Am Minerologist*. 1937;22:446–467.
11. Hartman P, Perdok WG. On the Relations between structure and morphology of crystals 1. *Acta Crystallographica*. 1955;8:49–52.
12. Hartman P, Bennema, P. The attachment energy as habit controlling factor. I. theoretical considerations. *J of Crystal Growth*. 1980;49: 145.
13. Berkovitch-Yellin Z. Toward an ab initio derivation of crystal morphology. *J Am Chem Soc*. 1985;107:8239–8253.
14. Hartman P. Structure and morphology. In: Hartman P, ed. *Crystal Growth: An Introduction*: North Holland, Amsterdam; 1973:367–402.
15. Clydesdale G, Roberts KJ, Lewtas K. Computational modeling study of the growth-morphology of the normal-alkane docosane and its mediation by tailor-made additives. *Molecular Crystals and Liquid Crystals Science and Technology Section a-Molecular Crystals and Liquid Crystals*. 1994;248:243–276.
16. Coombes DS, Catlow CRA, Gale JD, Hardy MJ, Saunders MR. Theoretical and experimental investigations on the morphology and pharmaceutical crystals. *J of Pharma Sci*. 2002;91:1652–1658.
17. Docherty R, Roberts KJ. Modeling the Morphology of Molecular-Crystals - Application to Anthracene, Biphenyl and Beta-Succinic Acid. *J of Crystal Growth*. 1988;88:159–168.
18. Liu XY, Bennema P. Prediction of the growth morphology of crystals. *J of Crystal Growth*. 1996;166:117–123.
19. Clydesdale G, Roberts KJ, Docherty R. Modeling the morphology of molecular-crystals in the presence of disruptive tailor-made Additives. *J of Crystal Growth*. 1994;135:331–340.
20. Clydesdale G, Roberts KJ, Lewtas K, Docherty R. Modeling the morphology of molecular-crystals in the presence of blocking tailor-made additives. *J of Crystal Growth*. 1994;141:443–450.
21. Bisker-Leib V, Doherty MF. Modeling the crystal shape of polar organic materials: Prediction of urea crystals grown from polar and nonpolar solvents. *Crystal Growth & Design*. 2001;1:455–461.
22. Bisker-Leib V, Doherty MF. Modeling crystal shape of polar organic materials: Applications to amino acids. *Crystal Growth & Design*. 2003;3:221–237.
23. Liu XY, Boek ES, Briels WJ, Bennema P. Prediction of crystal-growth morphology based on structural-analysis of the solid-fluid interface. *Nature*. 1995;374:342–345.
24. Winn D, Doherty MF. A new technique for predicting the shape of solution-grown organic crystals. *AIChE J*. 1998;44:2501–2514.
25. Winn D, Doherty MF. Predicting the shape of organic crystals grown from polar solvents. *Chem Eng Sci*. 2002;57:1805–1813.
26. Boerrigter SXM, Cuppen HM, Ristic RI, Sherwood JN, Bennema P, Meekes H. Explanation for the supersaturation-dependent morphology of monoclinic paracetamol. *Crystal Growth & Design*. 2002;2:357–361.
27. Sweegers C, Boerrigter SXM, Grimbergen RFP, Meekes H, Fleming S, Hiralal IDK, Rijkeboer A. Morphology prediction of gibbsite crystals - An explanation for the lozenge-shaped growth morphology. *J of Phys Chem B*. 2002;106:1004–1012.
28. Roberts KJ, Sherwood, JN, Yoon, CS and Docherty, R. Understanding the solvent-induced habit modification of benzophenone in terms of molecular recognition at the crystal/solution interface. *Chem of Mat*. 1994;6:1099–1102.
29. Liu XY, Bennema P. An inhomogeneous cell model and the growth of crystals. *J of Crystal Growth*. 1996;166:112–116.
30. Liu XY, Bennema P. Theoretical consideration of the growth morphology of crystals. *Phys Rev B*. 1996;53:2314–2325.
31. Gadewar SB, Doherty MF. A dynamic model for evolution of crystal shape. *J of Crystal Growth*. 2004;267:239–250.
32. Zhang YC, Sizemore JP, Doherty MF. Shape evolution of 3-dimensional faceted crystals. *AIChE J*. 2006;52:1906–1915.
33. Roberts KJ, Walker EM. Predicting particle morphology on the basis of the root molecular and crystal structure. *Current Opinion in Solid State and Materials*. 1996;1:506–513.
34. Rohl AL. Computer prediction of crystal morphology. *Current Opinion in Solid State & Mat Sci*. 2003;7:21–26.
35. Ramkrishna D. *Population balances-theory and applications to particulate systems in engineering*. San Diego: Academic Press; 2000.
36. Ramkrishna D, Mahoney AW. Population balance modeling. Promise for the future. *Chem Eng Sci*. 2002;57:595–606.
37. Campos FB, Lage PLC. A numerical method for solving the transient multidimensional population balance equation using an Euler-Lagrange formulation. *Chem Eng Sci*. 2003;58:2725–2744.
38. David R, Marchal P, Marcant B. Modeling of agglomeration in industrial crystallization from solution. *Chem Eng & Technol*. 1995;18:302–309.
39. Hulburt HM, Katz S. Some problems in particle technology - A statistical mechanical formulation. *Chem Eng Sci*. 1964;19:555–574.
40. Muhr H, David R, Villermaux J, Jezequel PH. Crystallization and precipitation engineering 6. Solving population balance in the case of the precipitation of silver bromide crystals with high primary nucleation rates by using the first order upwind differentiation. *Chem Eng Sci*. 1996;51:309–319.
41. Randolph A, Larson MA. *Theory of particulate processes: Analysis and techniques of continuous crystallization*. 2nd ed. Academic Press, London; 1988.
42. Garside J. Industrial crystallization from solution. *Chem Eng Sci*. 1985;40:3–26.
43. Franck R, David R, Villermaux J, Klein JP. Crystallization and precipitation engineering 2. a Chemical-reaction engineering approach to salicylic-acid precipitation - modeling of batch kinetics and application to continuous operation. *Chem Eng Sci*. 1988;43:69–77.
44. Marchal P, David R, Klein JP, Villermaux J. Crystallization and precipitation engineering 1. An efficient method for solving population balance in crystallization with agglomeration. *Chem Eng Sci*. 1988; 43:59–67.
45. Iveson SM. Limitations of one-dimensional population balance models of wet granulation processes. *Powder Technol*. 2002;124:219–229.
46. Puel F, Fevotte G, Klein JP. Simulation and analysis of industrial crystallization processes through multidimensional population balance equations. Part 1: a resolution algorithm based on the method of classes. *Chem Eng Sci*. 2003;58:3715–3727.
47. Puel F, Fevotte G, Klein JP. Simulation and analysis of industrial crystallization processes through multidimensional population balance equations. Part 2: a study of semi-batch crystallization. *Chem Eng Sci*. 2003;58:3729–3740.

48. Puel F, Marchal P, Klein J. Habit transient analysis in industrial crystallization using two dimensional crystal sizing technique. *Chem Eng Res & Des*. 1997;75:193–205.
49. David R, Villermaux J, Marchal P, Klein J-P. Crystallisation and percipitation engineering - IV. Kinetic model of adipic acid crystallisation. *Chem Eng Sci*. 1991;46:1129–1136.
50. Garside J. The concept of effectiveness factors in crystal growth. *Chem Eng Sci*. 1971;26:1425–1431.
51. Oullion M, Puel F, Fevotte G, Righini S, Carvin P. Industrial batch crystallization of a plate-like organic product. In situ monitoring and 2D-CSD modelling: Part 1: Experimental study. *Chem Eng Sci*. 2007;62:820–832.
52. Oullion M, Puel F, Fevotte G, Righini S, Carvin P. Industrial batch crystallization of a plate-like organic product. In situ monitoring and 2D-CSD modelling. Part 2: Kinetic modelling and identification. *Chem Eng Sci*. 2007;62:833–845.
53. Gerstlauer A, Gahn C, Zhou H, Rauls M, Schreiber M. Application of population balances in the chemical industry - current status and future needs. *Chem Eng Sci*. 2006;61:205–217.
54. Gerstlauer A, Mitrovic A, Motz S, Gilles ED. A population model for crystallization processes using two independent particle properties. *Chem Eng Sci*. 2001;56:2553–2565.
55. Gerstlauer A, Motz S, Mitrovic A, Gilles ED. Development, analysis and validation of population models for continuous and batch crystallizers. *Chem Eng Sci*. 2002;57:4311–4327.
56. Ma DL, Tafti DK, Braatz RD. High-resolution simulation of multidimensional crystal growth. *Ind & Eng Chem Res*. 2002;41:6217–6223.
57. Briesen H. Simulation of crystal size and shape by means of a reduced two-dimensional population balance model. *Chem Eng Sci*. 2006;61:104–112.
58. Zhang YC, Doherty MF. Simultaneous prediction of crystal shape and size for solution crystallization. *AIChE J*. 2004;50:2101–2112.
59. Clydesdale G, Thomson GB, Walker EM, Roberts KJ, Meenan P, Docherty R. A molecular modeling study of the crystal morphology of adipic acid and its habit modification by homologous impurities. *Crystal Growth & Design*. 2005;5:2154–2163.
60. Klapper H, Becker RA, Schmiemann D, Faber A. Growth-sector boundaries and growth-rate dispersion in potassium alum crystals. *Crystal Res and Technol*. 2002;37:747–757.
61. Ristic RI, Shekunov B, Sherwood JN. Long and short period growth rate variations in potash alum crystals. *J of Crystal Growth*. 1996;160:330–336.
62. Ristic RI, Shekunov BY, Sherwood JN. The influence of synchrotron radiation-induced strain on the growth and dissolution of brittle and ductile materials. *J of Crystal Growth*. 1997;179:205–212.
63. Lacmann R, Herden A, Mayer C. Kinetics of nucleation and crystal growth. *Chem Eng & Technol*. 1999;22:279–289.
64. Read WT, Shockley W. Dislocation Models of Crystal Grain Boundaries. *Physical Review*. 1950;78:275–289.
65. van der Heijden AEDM, van der Eerden JP. Growth-rate dispersion - the role of lattice strain. *J of Crystal Growth*. 1992;118:14–26.
66. Nollet S, Hilgers C, Urai JL. Experimental study of polycrystal growth from an advecting supersaturated fluid in a model fracture. *Geofluids*. 2006;6:185–200.
67. Synowietz C, Schafer, K. *Chemiker-Kalender*. Berlin: Springer; 1984.
68. Barrett P, Glennon B. Characterizing the metastable zone width and solubility curve using lasentec FBRM and PVM. *Chem Eng Res & Des*. 2002;80:799–805.
69. Matsuoka M, Abe Y, Uchida H, Takiyama H. Mechanism of growth rate enhancement by micro-crystals for the potash alum-water system. *Chem Eng Sci*. 2001;56:2325–2334.
70. Matsuoka M, Kamada T, Takiyama H. Growth rate enhancement of potash alum crystals by microcrystals. *J of Crystal Growth*. 1996;158:322–327.
71. Mullin JW, Garside J. Crystallization of aluminium potassium sulphate - a study in assessment of crystallizer design data I. - single crystal growth rates. *Trans of the Inst of Chem Eng and the Chem Eng*. 1967;45:T285–T290.
72. Hilgers C, Urai JL. Experimental study of syntaxial vein growth during lateral fluid flow in transmitted light: first results. *J of Structural Geology*. 2002;24:1029–1043.
73. Garside J. Kinetics of crystallisation form solution. In: Kaldis E, Scheel HJ., ed. *Crystal Growth and Materials*. North Holland, Amsterdam; 1977:484–513.
74. Calderon de Anda J, Wang XZ, Roberts KJ. Multi-scale segmentation image analysis for the in-process monitoring of particle shape with batch crystallisers. *Chem Eng Sci*. 2005;60:1053–1065.
75. Wang X, Calderon De Anda J, Roberts KJ, Li RF, Thomson GB, White G. Advances in on-line monitoring and control of the morphological and polymorphic forms of organic crystals grown from solution. *KONA*. 2005;23:69–85.
76. Wang XZ, Calderon De Anda J, Roberts KJ. Real-time measurement of the growth rates of individual crystal facets using imaging and image analysis: a feasibility study on needle-shaped crystals of L-glutamic acid. *Chem Eng Res & Des*. 2007;85:921–927.
77. Burton WK, Cabrera N, Frank FC. The growth of crystals and the equilibrium structure of their surfaces. *Philosophical Transactions of the Royal Society of London*. 1951;243:299–358.
78. Gilmer GH, Bennema P. Computer simulation of crystal surface-structure and growth kinetics. *J of Crystal Growth*. 1972;13/14:148–152.
79. Shampine LF, Watts, HA. Subroutine RKF45. In: G. E.Forsythe MAM, C. B.Moler, ed. *Computer Methods for Mathematical Computations*. Englewood Cliffs, N J.: Prentice-Hall; 1977:135–147.
80. Kumar S, Ramkrishna, D. On the solution of population balance equations by discretization - III. Nucleation, growth and aggregation of particles. *Chem. Eng Sci*. 1997;52:4659–4679.
81. Sun NF, Immanuel CD. Efficient solution of population balance models employing a hierarchical solution strategy based on a multilevel discretization. *Trans of the Inst of Measurement and Contr*. 2005;27:347–366.
82. Wettlaufer JS, Jackson M, Elbaums M. A geometric model for anisotropic crystal growth. *J Phys A: Math Gen*. 1994;27:5957–5967.
83. Amara N, Ratsimba, B, Wilhelm A., Delmas H. Growth rate of potash alum crystals: comparison of silent and ultrasonic conditions. *Ultrasonics Sonochemistry*. 2004;11:17–21.

Manuscript received Mar. 26, 2007, and revision received Sept. 24, 2007.